◎ 논 문

대류 및 소음 해석을 위한 정확한 다층 수치 기법

김 철 완*1

Accurate Multi-level Schemes for Advection and Acoustics

C. W. Kim

A non-dissipative and very accurate one-dimensional upwind leapfrog method is extended to higher-order and multi-dimensional advection and acoustic equations. The higher-order versions are developed by extending the stencils in space and time. The schemes are then successfully applied to the classical test cases for advection and acoustics.

Key Words: leapfrog, upwind, advection, acoustics, time reversible, non-dissipative

1. Introduction

Accurate numerical solutions of the scalar advection and acoustic equations are required in many contexts. Accuracy can be sought by several approaches. The simplest is to adopt increasingly higher-order interpolation, such as spectral analysis. This tends to produce very broad numerical stencils, especially if the temporal accuracy is obtained, as it often is, from higher-order time integration method such as Runge-Kutta. Another way to increase the data available for interpolation is to include information from more than one time-step. The simplest example is the leapfrog method, which is naturally non-dissipative and energy preserving. Leapfrog methods, however, have a poor reputation because spurious oscillations are pronounced, and the method often responds unstably to boundary conditions, mesh irregularity, or non-linear terms.

* 2003년 05월 27일 접수

*1 한국항공우주연구원

A variant of the leapfrog method was proposed by Iserles[1] for the one-dimensional (1D) advection equation, using stencil having only point symmetry and therefore the capability of reflecting an upwind bias. These have theoretical advantages over regular leapfrog methods, having much reduced phase error, more compact stencils and only positive group velocities. Therefore, the 1D equation has been extended to multi-dimensional system of equations (acoustics, Maxwell's equations, elastodynamics) by P. L. Roe[2]. In this paper, the 2D advection problem and acoustics are focused.

In Section 2, we briefly review the ideas of Iserles concerning three-level schemes, together with alternative methods of introducing additional information, such as the four-level and Hermitian schemes. The resolving power of these methods are remarkable, particularly those having 4th-order accuracy. The 4th-order three-level scheme yields less than 1% error with only four grid points per wavelength and less than 0.1% with

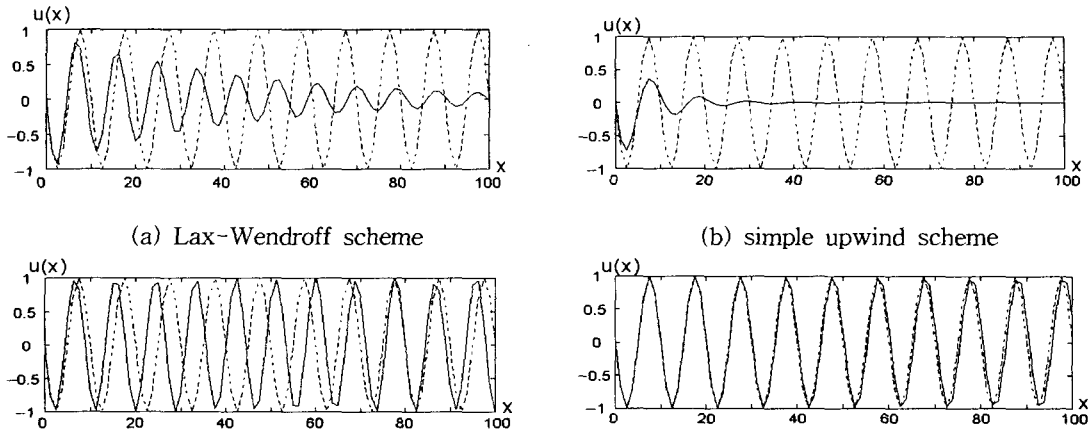

(a) Lax-Wendroff scheme (b) simple upwind scheme

(c) regular leapfrog scheme (d) upwind leapfrog scheme

Fig. 1 Numerical results of four different numerical scheme. Solid line: Numerical solution, Dotted line : Analytic solution. Courant No., $\nu = 0.4$. Grid points/wavelength, $N = 8$.

six points. Both four-level upwind leapfrog and Hermitian schemes yield less than 1% error with only three grid points per wavelength and less than 0.3% with five points. Therefore, these higher-order schemes are able to update the solution precisely for long integration times.

In Section 3, we discuss the strategies for extending these advection schemes to multi-dimensional advection and acoustic equations. The extension is not unique, but we follow heuristic principles of maintaining symmetry and minimizing the stencil. Both three-level and four-level methods are treated. Finally a couple of numerical experiments are demonstrated.

2. One-Dimensional Advection

The 1D advection equation for an unknown scalar $u(x, t)$, $\partial u/\partial t + a \cdot \partial u/\partial x = 0$, advects the given profile at the speed, a. Before any detailed analysis of the upwind leapfrog scheme, a few classical techniques are compared through simple numerical experiment. The left boundary of the computational domain is excited by a sinusoidal function which is propagated to the right-hand at the speed, a without any dissipation. Fig. 1 compares four different numerical test results with eight grid points per wavelength($N = 8$). Fig. 1(a) presents the result of the 2nd-order Lax-Wendroff scheme. After travelling only one wavelength (ten iterations), it begins to show some deviation from the analytic solution (dotted line) and produces substantial dispersion and dissipation errors after travelling ten wavelengths(200 iterations). Fig. 1(b) is updated by the simple upwind scheme which has a huge dissipation error and shows that most of the amplitude is dissipated after travelling three wavelengths. Neither of these schemes is suitable for accurately simulating advection, and would require more grid points to get a reasonable result.

The third picture, Fig. 1(c), is obtained with the regular leapfrog scheme, which uses three level and is time-reversible(Fig. 3). Therefore, it has no dissipation and maintains the original amplitude. However, it has a large dispersion error and still requires a lot more grid to get reasonable phase resolution. The last picture (Fig. 1(d)) shows the result of the upwind leapfrog scheme proposed by Iserles[1]. It is again time-reversible and keeps the original wave amplitude without any dissipation.

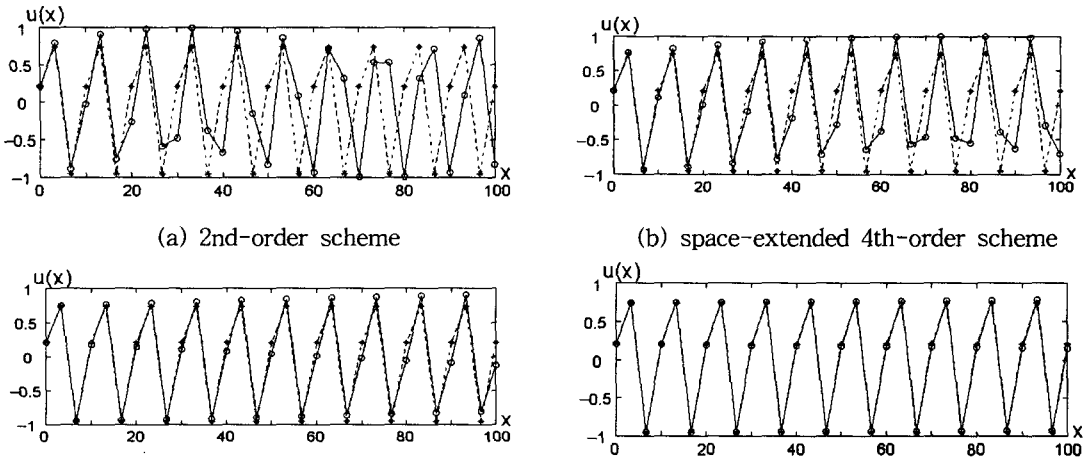

Fig. 2 Numerical results of four upwind leapfrog schemes. Solid line and circle : Nu-merical solution. Dotted line and star: Analytic solution. Courant No, ν (a),(b)=0.4, (c),(d)=0.2. Grid points/wavelength, $N=3$.

Furthermore the biased stencil maintains the phase very precisely.

Another experiment, shown in Fig. 2 demonstrated the accuracy of the 2nd-, 4th- and 6th-order upwind leapfrog methods on a coarse grid, $N=3$. Although the analytic solution, marked by star(*) and dotted line, is a smooth sine wave, the interpolation of the analytic solution appears discrete. The result of the 2nd-order scheme shown in Fig. 2(a) begins to show a dispersion error after travelling one wavelength. Two 4th-order schemes developed by extending the 2nd-order scheme in space and time, demonstrate the results in Fig. 2(b) and 2(c). They preserve the phase precisely. However, to graphical resolution, the method using the time-extended stencil is more accurate than the one extended in space. As heuristic reason for it being better than the stencil extended in space is that it has a smaller extent in the characteristic coordinate $x-at$. The 6th-order scheme based on the stencil shown in Fig. 4(c) preserves the phase with extraordinary accuracy for such an under-resolved grid. In

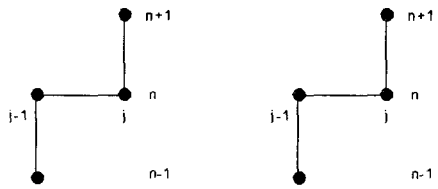

Fig. 3 Stencils of leapfrog type schemes. left : regular leapfrog, right : upwind leapfrog

what follows, we successfully extend both 4th-order methods to 2D grids; extension of the corresponding sixth-order version remains to be achieved.

2.1. 2nd-order upwind leapfrog scheme

For positive wave speed, $a>0$, the regular leapfrog and upwind leapfrog schemes employ the stencils of Fig. 3 and are time-reversible.

Regular leapfrog :

$$u_j^{n+1} = u_j^{n-1} - \nu(u_{j+1}^n - u_{j-1}^n), \quad (1)$$

Upwind leapfrog :

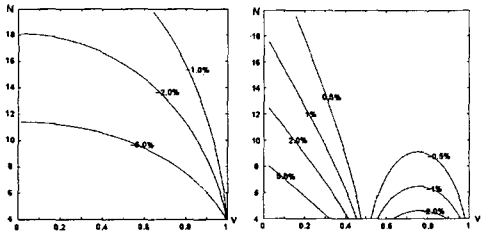

(a) Regular Leapfrog (b) Upwind Leapfrog

Fig. 4 Phase properties of 2nd order leap-frog scheme

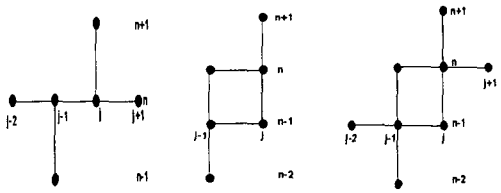

(a) (b) (c)

Fig. 5 Stencils of the 4th- and sixth-order upwind leapfrog schemes. (a) space-extended 4th-order, (b) time-extended 4th-order, (c) space- and time-extended sixth order.

$$u_j^{n+1} = u_{j-1}^{n-1} + (1-2\nu)(u_j^n - u_{j-1}^n), \qquad (2)$$

where $\nu = a\Delta t/\Delta x$.

For the analysis of two schemes, von Neumann analysis is performed. The results are presented as contour plots of equal phase error, on diagrams where the axes are $\nu(\geqq 0)$ and $N(\geqq 2)$. The results for the regular and upwind leapfrog scheme are shown in Fig. 4

2.2 Higher-order upwind leapfrog

To get higher-order accuracy, more data is necessary beyond that used in the 2nd-order upwind leapfrog scheme. To provide the information, the stencil is extended in space or time. The first is to extend the stencil of the 2nd-order scheme in space, as shown in Fig. 5(a) but this makes the scheme less compact and is difficult to apply at the boundary. The second is to stretch the stencil in time by including data from time level $n-2$ (Fig. 5(b)). This results in a very accurate scheme that is exact both when $\nu=1/2$ and when $\nu=1/3$. However, this scheme is unstable for $\nu>1/2$. Another method is to combine these methods. Fig. 5(c) shows the stencil of the sixth-order scheme obtained by extending the 2nd-order stencil in space and time.

Space-extended 4th order scheme, Fig 5(a)

$$u_j^{n+1} = u_{j-1}^{n-1} + \frac{(\nu+1)(2\nu^2-5\nu+2)}{2}(u_j^n - u_{j-1}^n) - \frac{\nu(\nu-1)(2\nu-1)}{6}(u_{j+1}^n - u_{j-2}^n) \qquad (3)$$

Time-extended 4th order scheme, Fig. 5(b)

$$u_j^{n+1} = u_{j-1}^{n-2} + 2(1-3\nu)(u_j^n - u_{j-1}^{n-1}) + \frac{(1-2\nu)(1-3\nu)}{\nu+1}(u_{j-1}^n - u_j^{n-1}) \qquad (4)$$

Time/Space-extended 6th-order scheme, Fig. 5(c)

$$u_j^{n+1} = u_{j-1}^{n-2} - 4\frac{(3\nu-1)(\nu^2-1)}{\nu-2}(u_j^n - u_{j-1}^{n-1}) - (6\nu^2-5\nu+1)(u_j^{n-1} - u_{j-1}^n) + \frac{\nu^2(6\nu^2-5\nu+1)}{\nu^2-5\nu+6}(u_{j+1}^n - u_{j-2}^{n-1}) \qquad (5)$$

3. 2-Dimensional Upwind Leapfrog Schemes

2nd-order upwind leapfrog schemes for advection and acoustic equations are presented in this section.

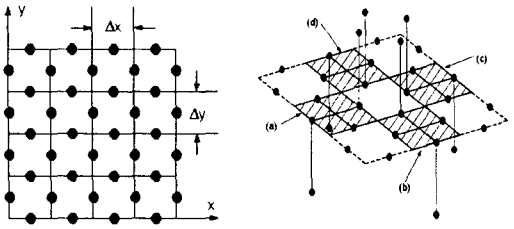

Fig. 6 Staggered grid arrangement and stencils of the 2nd-order schemes

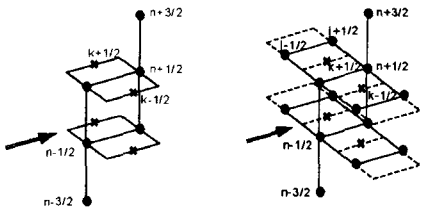

Fig. 7 Four-level 2nd- and 4th-order stencils on staggered grid

3.1. 2nd-order advection schemes

The 2D advection equation is

$$\frac{\partial u}{\partial t}+a\frac{\partial u}{\partial x}+b\frac{\partial u}{\partial y}=0 \tag{6}$$

and the advection speed, (a,b) is assumed to be constant. The propagation direction, α, is defined as $\alpha=\tan^{-1}(b/a)$. There are a few approaches to extend the upwind leapfrog method to multi-dimensions. They primarily depend on the computational grid type as mentioned by Roe and Thomas[4,5]. To be consistent with the mesh arrangement of the acoustic schemes, staggered grid storing the variable at the cell edge, is utilized. Although the staggered grid is merely a scaling and rotation of the uniform grid, they are generally treated distinctly because in wave propagation problems, it is sometimes advantageous to store different variables at different nodes of the staggered mesh.

The 2nd-order stencils are shown in Fig. 6 and the discretized equations are

$$\text{a) } \delta_t u^{n+\frac{1}{2}}_{j+\frac{1}{2},k}+\delta_t u^{n-\frac{1}{2}}_{j-\frac{1}{2},k}+2\nu_x\delta_x u^n_{j,k}+2\nu_y\delta_y u^n_{j,k}=0 \tag{7}$$

$$\text{b) } \delta_t u^{n+\frac{1}{2}}_{j,k+\frac{1}{2}}+\delta_t u^{n-\frac{1}{2}}_{j,k-\frac{1}{2}}+2\nu_x\delta_x u^n_{j,k}+2\nu_y\delta_y u^n_{j,k}=0 \tag{8}$$

$$\text{c) } \delta_t u^{n+\frac{1}{2}}_{j-\frac{1}{2},k}+\delta_t u^{n-\frac{1}{2}}_{j+\frac{1}{2},k}+2\nu_x\delta_x u^n_{j,k}+2\nu_y\delta_y u^n_{j,k}=0 \tag{9}$$

$$\text{d) } \delta_t u^{n+\frac{1}{2}}_{j,k-\frac{1}{2}}+\delta_t u^{n-\frac{1}{2}}_{j,k+\frac{1}{2}}+2\nu_x\delta_x u^n_{j,k}+2\nu_y\delta_y u^n_{j,k}=0 \tag{10}$$

where $\nu_x=a\Delta t/\Delta x$, $\nu_y=b\Delta t/\Delta y$ and the discrete differencing and averaging operators are defined by

$$\delta_t u^n_{j,k}=u^{n+\frac{1}{2}}_{j,k}-u^{n-\frac{1}{2}}_{j,k}, \qquad \mu_t u^n_{j,k}=\frac{u^{n+\frac{1}{2}}_{j,k}+u^{n-\frac{1}{2}}_{j,k}}{2},$$

$$\delta_x u^n_{j,k}=u^n_{j+\frac{1}{2},k}-u^n_{j-\frac{1}{2},k}, \qquad \mu_x u^n_{j,k}=\frac{u^n_{j+\frac{1}{2},k}+u^n_{j-\frac{1}{2},k}}{2},$$

$$\delta_y u^n_{j,k}=u^n_{j,k+\frac{1}{2}}-u^n_{j,k-\frac{1}{2}}, \qquad \mu_y u^n_{j,k}=\frac{u^n_{j,k+\frac{1}{2}}+u^n_{j,k-\frac{1}{2}}}{2}.$$

We will adopt whichever of (a), (b), (c) or (d) respects the domain of dependence. This means that the solution may not depend continuously on the direction of propagation, and for computing steady-state solutions this might cause problems with convergence. However, we have not found any difficulties due to this dependence in the linear scalar case.

3.2 Higher-order advection schemes

To develop schemes of 4th-order accuracy, the stencil of the 2nd-order method is extended into time. The 2nd-order truncation error terms of the upwind leapfrog scheme are presented as

$$\delta_t u^{n+1}_{j+\frac{1}{2},k} + \delta_t u^{n-1}_{j-\frac{1}{2},k} + 2(\nu_x\delta_x + \nu_y\delta_y)\mu_t u^n_{j,k} = 2\Delta t$$

$$(\frac{\partial u}{\partial t} + a\frac{\partial u}{\partial x} + b\frac{\partial u}{\partial y}) + \frac{\Delta x^2\Delta t}{12}[a\frac{\partial^3 u}{\partial x^3} + b\frac{\Delta y^2}{\Delta x^2}\frac{\partial^3 u}{\partial y^3}$$

$$3\frac{\partial^3 u}{\partial x^2\partial t} + 12\frac{\Delta t}{\Delta x}\frac{\partial^3 u}{\partial x\partial t^2} + 10\frac{\Delta t^2}{\Delta x^2}\frac{\partial^3 u}{\partial t^3}] + O(\Delta x^4)\,.$$

The four-level compact stencil shown in Fig. 7 is not enough to eliminate the 2nd-order errors and the smallest stencil on which the error terms could be discretized, is presented in Fig. 7(b). With the relation, $\partial u/\partial t = -a\partial u/\partial x - b\partial u/\partial y$, some terms are replaced as below because they could not be discretized on the stencil(Fig. 7(b)). Then the error terms are discretized and the resultant scheme is

$$\begin{aligned}&\delta_t u^{n+1}_{j+\frac{1}{2},k} + \delta_t u^{n-1}_{j-\frac{1}{2},k} + 2(\nu_x\delta_x + \nu_y\delta_y)\mu_t u^n_{j,k}\\ &-\{c_{xyy}\mu_t\delta_x\delta_y^2 + c_{xxt}[8\delta_t(\mu_x - \mu_y) + \delta_y^2\delta_t\mu_x]\\ &+c_{xyt}\delta_t\mu_y\delta_y\delta_x + c_{yyt}\delta_y^2\delta_t\mu_x\}u^n_{j,k} = 0\end{aligned} \tag{11}$$

where

$$c_{xyy} = \frac{\nu_y^2 - \nu_x^2}{12\nu_x}, \qquad c_{xxt} = \frac{(10\nu_x - 2)(\nu_x - 1)}{12}$$

$$c_{xyt} = \frac{\nu_y(10\nu_x - 1)(2\nu_x - 1)}{12\nu_x}, \qquad c_{yyt} = \frac{10\nu_y^2 - 1}{12}$$

3.3. 2nd-order acoustics schemes

Multi-dimensional acoustics is represented by the linearized Euler equations. These equations having pressure and velocity fluctuations(p, $\boldsymbol{u} = [u, v, w]$) are

$$\begin{aligned}&p_t + \rho_o a_o^2 \nabla \cdot \boldsymbol{u} = 0,\\ &\boldsymbol{u}_t + \frac{1}{\rho_o}\nabla p = 0,\end{aligned} \tag{12}$$

where ρ_o and a_o are steady state values of density and speed of sound. To develop the upwid leapfrog method for acoustics, the system of equations (12) is arranged in characteristic form which is as similar as possible to the advection equation, because characteristic form of equations clarifies wave propagation direction. Characteristic equations aligned along x- and y-axis are used as the governing equations of two-dimensional acoustics and expressed as follows.

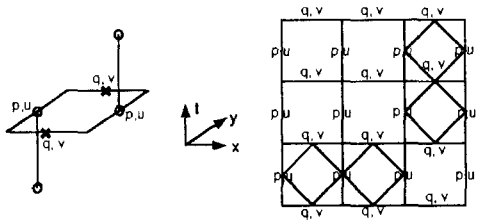

Fig. 8 Stencils of 2nd-order upwind leapfrog methods.

$$\begin{aligned}&(\frac{\partial}{\partial t} \pm a_o\frac{\partial}{\partial x})(p \pm \rho_o a_o u) = -\rho_o a_o^2\frac{\partial v}{\partial y},\\ &(\frac{\partial}{\partial t} \pm a_o\frac{\partial}{\partial y})(p \pm \rho_o a_o v) = -\rho_o a_o^2\frac{\partial u}{\partial x}.\end{aligned} \tag{13}$$

Since the left-hand sides of the above equations resemble one-dimensional advection equation, they can be discretized in the same way as the one-dimensional scheme. The right-hand sides are discretized by central differencing. As a typical difficulty encountered in application of characteristic equations, three unknown variables should be updated in two-dimensional acoustics although the characteristic method provides four relations and the pressure is updated twice.

The staggered grid method storing the variables as showin in Fig. 8, was developed by Roe and Thomas[3] to discretize the characteristic equation without dissipation. The pressure updated with u is stored with u and the other pressure with v is stored with v. The pressure updated with v is described as q and ρ_o and a_o are set to unity for convenience. Therefore, the characteristic equations are

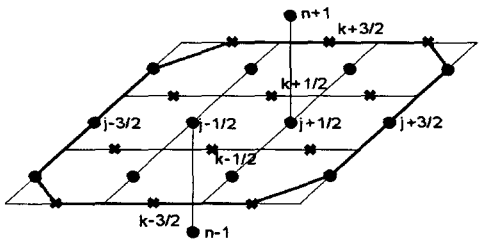

Fig. 9 3-level 4th-order stencil for +x wave

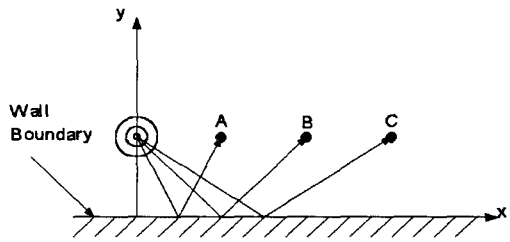

Fig. 10 Explanation of initial value problem for comparison of leapfrog type schemes

$$\frac{\partial}{\partial t}(p\pm u)\pm\frac{\partial}{\partial x}(p\pm u)=-\frac{\partial v}{\partial y}\,,\qquad \frac{\partial}{\partial t}(q\pm v)\pm\frac{\partial}{\partial y}(q\pm v)=-\frac{\partial u}{\partial x}\,. \tag{14}$$

and discretized as follows.

$$\begin{aligned}
&\delta_t(p+u)^{n+\frac12}_{j+\frac12,k}+\delta_t(p+u)^{n-\frac12}_{j-\frac12,k}\\
&\qquad+2\nu_x\delta_x(p+u)^n_{j,k}+2\nu_y\delta_y v^n_{j,k}=0,\\
&\delta_t(p-u)^{n+\frac12}_{j-\frac12,k}+\delta_t(p-u)^{n-\frac12}_{j+\frac12,k}\\
&\qquad-2\nu_x\delta_x(p-u)^n_{j,k}+2\nu_y\delta_y v^n_{j,k}=0,\\
&\delta_t(q+v)^{n+\frac12}_{j,k+\frac12}+\delta_t(q+v)^{n-\frac12}_{j,k-\frac12}\\
&\qquad+2\nu_y\delta_y(q+v)^n_{j,k}+2\nu_x\delta_x u^n_{j,k}=0,\\
&\delta_t(q-v)^{n+\frac12}_{j,k-\frac12}+\delta_t(q-v)^{n-\frac12}_{j,k+\frac12}\\
&\qquad-2\nu_y\delta_y(q-v)^n_{j,k}+2\nu_x\delta_x u^n_{j,k}=0.
\end{aligned} \tag{15}$$

This method eliminates the averaging of pressures and updates solutions without any dissipation. Furthermore, the staggered grid provides compact stencil, which is considered as another advantage of the staggered grid.

3.4. Higher-order acoustics schemes

To develop higher-order scheme, the stencil of the second-order scheme, Fig. 8 is extended in space as shown in Fig. 9. Developing a three-level fourth-order scheme would be straightforward if stability were not an issue. The second-order scheme for $(p+u)$ wave with the second-order error terms is

$$\begin{aligned}
&\delta_t(p+u)^{n+\frac12}_{j+\frac12,k}+\delta_t(p+u)^{n-\frac12}_{j-\frac12,k}+2\delta_x(p+u)^n_{j,k}+2\delta_y v^n_{j,k}=\\
&-c_{p_{xxx}}\Delta x^3\frac{\partial^3 p}{\partial x^3}-c_{q_{xxy}}\Delta x\Delta y^2\frac{\partial^3 q}{\partial x\partial y^2}-c_{u_{xxx}}\Delta x^3\frac{\partial^3 u}{\partial x^3}\\
&-c_{u_{xxy}}\Delta x\Delta y^2\frac{\partial^3 u}{\partial x\partial y^2}-c_{v_{xxy}}\Delta x^2\Delta y\frac{\partial^3 v}{\partial x^2\partial y}-c_{v_{xyy}}\Delta y^3\frac{\partial^3 v}{\partial y^3},
\end{aligned} \tag{16}$$

where

$$\begin{aligned}
&c_{p_{xxx}}=\frac16(2\nu_x^3-3\nu_x^2+\nu_x), \qquad c_{q_{xxy}}=\frac23\nu_y^2(2\nu_x-3),\\
&c_{u_{xxx}}=\frac16(2\nu_x^3-3\nu_x^2+\nu_x), \qquad c_{u_{xyy}}=\frac13\nu_x\nu_y^2\,,\\
&c_{v_{xxy}}=\frac{1}{12}\nu_y(4\nu_x^2-6\nu_x+3), \qquad c_{v_{yyy}}=\frac{1}{12}\nu_y(4\nu_y^2-1).
\end{aligned}$$

Then discretizing the second-order errors and moving them to the left hand side increase the order of accuracy. The discretizations of the error terms are as follows.

$$\begin{aligned}
&\Delta x^3\frac{\partial^3 p}{\partial x^3}=\delta_x^3 p^n_{j,k}, \qquad \Delta x^3\frac{\partial^3 u}{\partial x^3}=\delta_x^3 u^n_{j,k}\,,\\
&\Delta y^3\frac{\partial^3 v}{\partial y^3}=\delta_y^3 v^n_{j,k}, \qquad \Delta x\Delta y^2\frac{\partial^3 q}{\partial x\partial y^2}=\mu_x\mu_y\delta_x\delta_y^2 q^n_{j,k},\\
&\Delta x\Delta y^2\frac{\partial^3 u}{\partial x\partial y^2}=\frac{1}{24}(28\delta_x\delta_y^2-4\mu_x^2\delta_x\delta_y^2)u^n_{j,k},\\
&\Delta x^2\Delta y\frac{\partial^3 v}{\partial x^2\partial y}=\frac{1}{24}(28\delta_x^2\delta_y-4\mu_y^2\delta_x^2\delta_y)v^n_{j,k}.
\end{aligned}$$

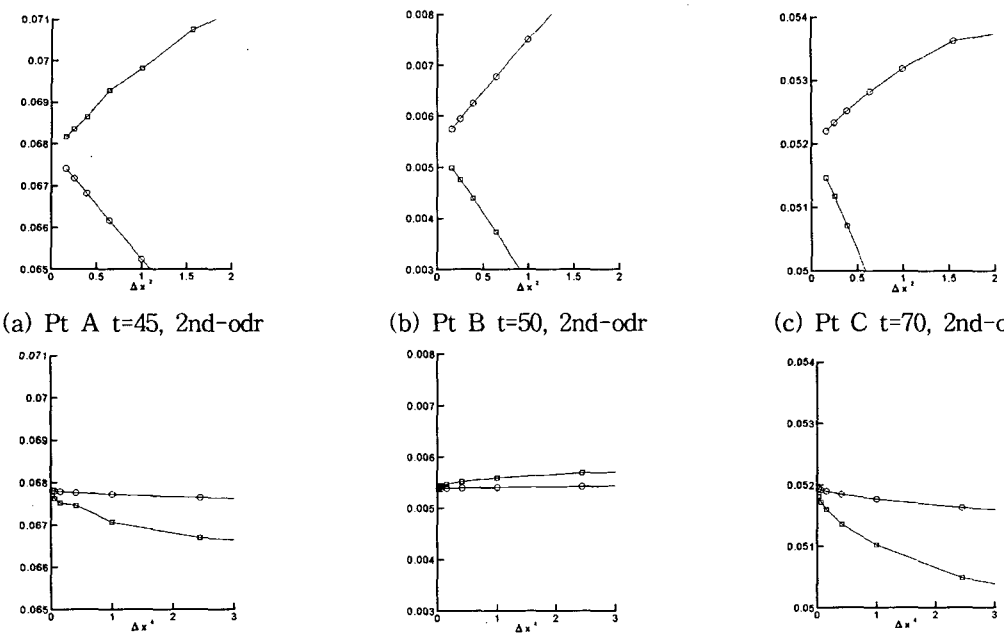

(a) Pt A t=45, 2nd-odr (b) Pt B t=50, 2nd-odr (c) Pt C t=70, 2nd-odr

(d) Pt A t=45, 4th-odr (e) Pt B t=50, 4th-odr (f) Pt C t=70, 4th-odr

Fig. 11 Grid convergence histories, circle : upwind leapfrog, square : Yee's standard leapfrog method

Other characteristics equations can be discretized in the way described above.

3.5. Accuracy Comparison of Leapfrog Schemes

Another leapfrog type scheme is Yee's standard leapfrog scheme, mainly designed for electromagnetics and acoustics. It stores pressure and velocities at cell center and edges respectively. Its accuracy is comparable to the upwind leapfrog method. Nguyen[6] compared phase properties of these schemes and concluded that floating point operations per cell of two-dimensional second-order upwind leapfrog method is more than that of Yee's scheme but its accuracy is higher than Yee's schems. Therefore the efficiency of both schemes are comparable. To confirm that comparison, a simple initial value problem is devised as shown in Fig. 10.

Initial values are

$$p(x, y) = \exp\left(-\frac{\ln 2}{5^2}[x^2+(y-20)^2]\right),$$

$$u(x, y) = v(x, y) = 0.$$

The positions of the points A, B and C are (20,20), (40,20) and (60,20). Ghost cells are generated with mirror images for wall boundary treatment and the Courant numbers (ν_x, ν_y) are 1/4. Pressure values are measured at each point and compared on various grid sizes.

Measuring time of the points A, B and C are 45, 50 and 70. Fig. 11 presents the grid convergence histories of each point. The results of the second-order schemes(Fig. 11(a), (b) and (c)) show very similar accuracy level. However, the fourth-order results (Fig. 11(d), (e) and (f)) demonstrate distinct deviation between two results. The fourth-order upwind leapfrog scheme updates accurate solutions

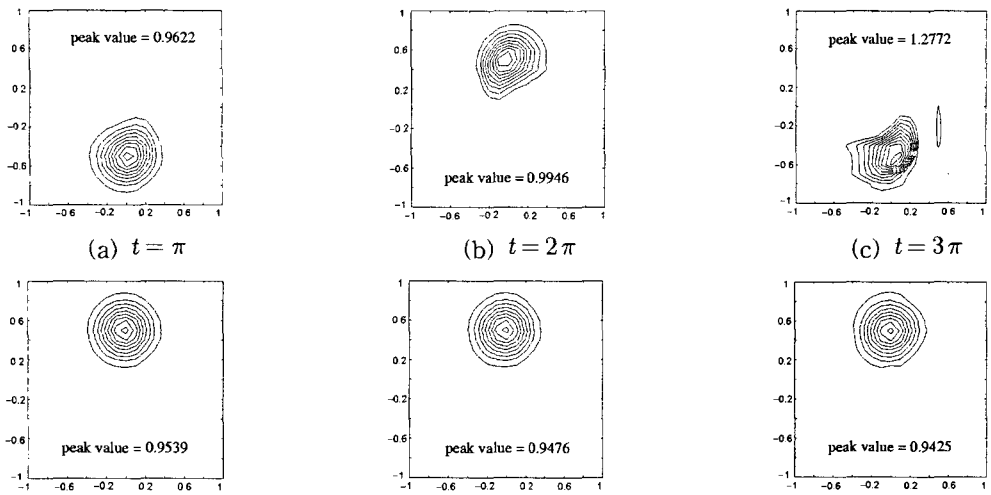

(a) $t=\pi$ (b) $t=2\pi$ (c) $t=3\pi$

(d) $t=2\pi$ (e) $t=4\pi$ (f) $t=8\pi$

Fig. 12 Rotating disk simulation with the upwind leapfrog methods. Grid size = 20x20. (a),(b),(c):2nd-order, (d),(e),(f): 4th-order.

with even coarse grid.

4. Numerical Experiments

The 2nd- and 4th-order upwind leapfrog schemes for advection and the 2nd-order acoustic equations are applied to typical test examples such as rotating disk and piston problem simulation.

4.1. Rotating Disk

We consider the case of advection in a circle, governed by the equation

$$\frac{\partial u}{\partial t} + y\frac{\partial u}{\partial x} - x\frac{\partial u}{\partial y} = 0 \quad . \qquad (17)$$

Fig. 12 presents the results of simulating the above equation (17) with the 2nd-order and 4th-order schemes on 20x20 grid. With the 2nd-order scheme, the distribution starts to distort after one revolution(Fig. 12(a)). the solution does not preserve the initial shape after one revolution, Fig. 12(b) and the measured peak values are meaningless, Fig. 12(b)-(c).

The 4th-order scheme is applied with some additional terms to achieve the resolution. The additional term for the +x-axis is

$$-(c_{xx}\delta_x^2 + c_{xy}\delta_x\delta_y + c_{yy}\delta_y^2 + c_{xt}\delta_x\delta_t + c_{yt}\delta_y\delta_t)u_{j,k}^n$$

where

$$c_{xx} = -\bar{\nu}_y\delta_y\bar{\nu}_x/12\bar{\nu}_x, \quad c_{xy} = (\delta_y\bar{\nu}_x + \delta_x\bar{\nu}_y)/6,$$
$$c_{yy} = -\bar{\nu}_y\delta_x\bar{\nu}_y/12\bar{\nu}_x, \quad c_{xt} = -5\bar{\nu}_y\delta_y\bar{\nu}_x/12,$$
$$c_{yt} = (6-5\bar{\nu}_x)\delta_x\bar{\nu}_y/12$$

and $\bar{\nu}_x = \nu_x|_{j,k}$, $\bar{\nu}_y = \nu_y|_{j,k}$. Those terms are discretized and subtracted from the four-level scheme(11). This correction improves the resolution and leads to the results shown in Fig. 12(d)-(f). The 4th-order scheme does not change the initial distribution and generate any disturbance. Even four revolution does not distort the initial distribution and its peak value decreases steadily by 5.75% over the course of evolution.

4.2. Piston Problem Simulation

The acoustic wave produced by an

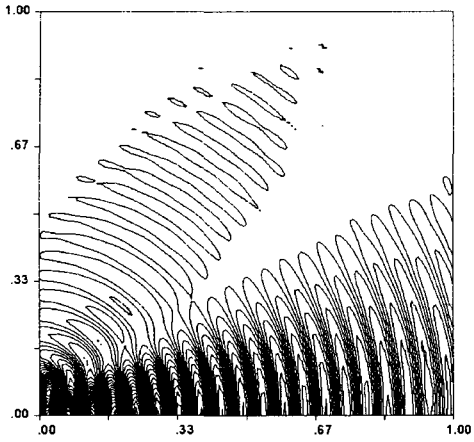

Fig. 13 Pressure contour plot of Piston Problem. $\Delta x = \Delta y = 1/12, t = 3.0$.

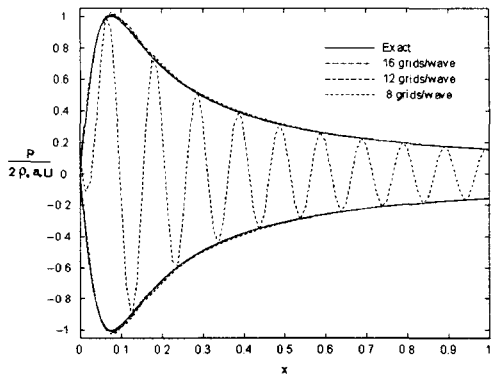

Fig. 14 Comparison of numerical pressure envelopes with analytic solution for various grid sizes.

oscillating piston with an axisymmetric infinite baffle(Fig. 13) was simulated to test the numerical scheme. This problem is governed by the linearized axisymmetric Euler equations whose characteristic form is

$$\frac{\partial}{\partial t}(p \pm u) \pm \frac{\partial}{\partial x}(p \pm u) + \frac{\partial v}{\partial y} = -\frac{v}{y}\,,$$
$$\frac{\partial}{\partial t}(q \pm v) \pm \frac{\partial}{\partial y}(q \pm v) + \frac{\partial u}{\partial x} = -\frac{v}{y}\,. \qquad (18)$$

The analytic solution for the magnitude of the pressure oscillations along the axis of symmetry[9] is given as

$$\frac{P(x)}{2\rho_o a_o U} = \left|\sin\left(\frac{\pi f x}{a_o}\left[\sqrt{1+\left(\frac{r_o^2}{x}\right)^2}-1\right]\right)\right|\,, \qquad (19)$$

where P is the magnitude of pressure oscillation, U is the piston displacement magnitude, f is the frequency and r_o is its radius. Equation(19) shows that the axial pressure magnitude is function of f, r_o and x for given $\rho_o a_o$ and U. For simplicity, $\rho_o a_o$ and U are set to one. The axisymmetric equations also have a source term, $-v/y$ which is independent of $(p \pm u)$ and it was discretized by central differencing. However the source term of Equation(18) is dependent on $(q \pm v)$ and it requires a stabilizing technique described in [8]. Three-level 2nd-order upwind leapfrog schemes were implemented for this experiment. The frequency is chosen as ten cycles per unit time and r_o equal to 1/10 of unit length. The computational domain is $0 \leqq x \leqq 1.0$ and $0 \leqq y \leqq 1.0$. Fig. 13 shows the contour plot of acoustic field. The grid size used for this computation and the Courant number were 120x120 and 1/2 respectively. Most of the acoustic energy was transmitted along the axis of symmetry and a smaller portion was radiated diagonally. Giles' 2nd-order boundary condition was implemented at the far-field and little outgoing acoustic wave was reflected. Pressure magnitudes along the axis were compared with the analytic solution for various grid size in Fig. 14 and the result exhibits good agreement with the analytic solution even on the coarse grid (8 cells per wavelength). As the grid is refined, numerical results converged to the analytic solution.

5. Conclusion

One-dimensional version of the upwind leapfrog method was successfully extended to multi-dimensional advection and acoustic equations. This work is an attempt at creating highly accurate schemes for passive advection of scalar quantity. By design, these methods are free from dissipation and the dispersion error could be reduced significantly by keeping the stencil compact in the characteristic coordinate. Numerical experiment results assure the accuracy of the upwind leapfrog method.

References

[1] Iserles, A, "Generalized leapfrog method," *IMA Journal of Numerical Analysis,* (1986).

[2] Roe, P. L., "Linear Characteristic Schemes without Dissipation," *SIAM Journal on Scientific Computing* (1998) 19(5):1405-1427

[3] Thomas, J. P., Roe, P. L., "Development of non-dissipative numerical schemes for computational aeroacoustics," *AIAA Paper 93-3382, AIAA 11th CFD Conf.,* (1993).

[4] Thomas, J. P., Kim, C. and Roe, P. L., "Progress towards a new computational scheme for aeroacoustics," *AIAA Paper 95-1758, AIAA 12th Computational Fluid Dynamics Conference,* (1995).

[5] Thomas, J. P. *Ph. D. Thesis,* Department of Aerospace Engineering, University of Michigan, (1996).

[6] Nguyen, B. T. *Ph. D. Thesis,* Department of Aerospace Engineering, University of Michigan, (1996).

[7] Kim, C., Thomas, J. P. and Roe, P. L., "Accurate Schemes for Advection and Aeroacoustics," *AIAA Paper 97-2091, AIAA 13th CFD Conference,* (1997).

[8] Kim, C., "Maintaining the stability of a leapfrog scheme in the presence of source terms", International Journal for Numerical Methods in Fluids, (2003), 42:839-852

[9] Kinsler, L. E., Frey, A. R., Coppens, A. B., and Sanders, J. V., *Fundamentals of Acoustics,* 3rd edition, John Wiley & Sons